New Journal of Physics
The open-access journal for physics

Particle–wave discrimination in Poisson spot experiments

T Reisinger[1,3], G Bracco[1,2] and B Holst[1]

[1] Department of Physics and Technology, University of Bergen, Allegaten 55, 5007 Bergen, Norway
[2] CNR-IMEM, Department of Physics, University of Genova, V Dodecanesco 33, 16146 Genova, Italy
E-mail: treisinger@gmail.com

New Journal of Physics **13** (2011) 065016 (13pp)
Received 20 December 2010
Published 28 June 2011
Online at http://www.njp.org/
doi:10.1088/1367-2630/13/6/065016

Abstract. Matter–wave interferometry has been used extensively over the last few years to demonstrate the quantum-mechanical wave nature of increasingly larger and more massive particles. We have recently suggested the use of the historical Poisson spot setup to test the diffraction properties of larger objects. In this paper, we present the results of a classical particle van der Waals (vdW) force model for a Poisson spot experimental setup and compare these to Fresnel diffraction calculations with a vdW phase term. We include the effect of disc-edge roughness in both models. Calculations are performed with D_2 and with C_{70} using realistic parameters. We find that the sensitivity of the on-axis interference/focus spot to disc-edge roughness is very different in the two cases. We conclude that by measuring the intensity on the optical axis as a function of disc-edge roughness, it can be determined whether the objects behave as de Broglie waves or classical particles. The scaling of the Poisson spot experiment to larger molecular masses is, however, not as favorable as in the case of near-field light-grating-based interferometers. Instead, we discuss the possibility of studying the Casimir–Polder potential using the Poisson spot setup.

[3] Author to whom any correspondence should be addressed.

Contents

1. Introduction

In the Poisson spot diffraction experiment, an object with a circular rim, such as a sphere or a circular disc, casts a shadow with a bright interference spot at its center [1, 2]. See figure 2 for a diagram of the experimental setup in a Poisson spot experiment. This bright spot is due to positive wave interference stemming from the fact that all paths from the source to the bright spot via the rim have the same length. It convincingly demonstrated the wave nature of light at the beginning of the 19th century, as the bright spot was interpreted as clearly contradicting the straight-line propagation expected from classical particles.

There is plenty of experimental evidence for the wave nature of material particles as conjectured in Louis de Broglie's hypothesis [3]. In the Fraunhofer regime, we find, for example, Davisson and Germer's famous electron-diffraction experiments using nickel crystals [4]. The Fresnel fringes from a one-dimensional (1D) Poisson spot experiment that makes use of a wire instead of a circular disc can be readily observed in transmission electron microscopes equipped with a biprism for electron holography [5]. Also, diffraction from a zone plate can be interpreted as a more complex application of the Poisson spot principle and has been performed with, for example, neutrons [6], neutral atoms [7–9] and molecules [10]. We have recently performed the first classical Poisson spot experiment with neutral matter waves, using the diatomic molecule deuterium (D_2) [11], and argued that it is scalable to work with molecules of higher mass and complexity. In this paper, we further explore this idea and the role of van der Waals (vdW) interaction between the passing molecules and the circular obstacle. The latter point is important because the vdW attraction also leads to an intensity peak at the center of the obstacle shadow [12].

The demonstration of quantum-mechanical interference of larger molecules is motivated by, among others, the desire to understand the transition from the quantum-mechanical regime to the classic regime. One of the most prominent experiments was the far-field-grating diffraction experiment with the fullerene C_{60} [13]. This has since progressed to experiments with near-field Kapitza–Dirac–Talbot–Lau interferometers [14], demonstrating matter–wave interference for particles as massive as 1632 atomic mass units. Apart from fundamental physics, there are several other applications for such matter–wave interference experiments [15]; for example, molecule lithography [16], mass spectrometry [17] and the measurement of dispersion forces [18]. Below we will specifically discuss the latter in the context of the Poisson spot experiment.

To clearly distinguish between classical particle behavior and quantum-mechanical wave nature in the Poisson spot experiment with molecules, it is important to consider the attractive

vdW potential that is experienced by polarizable particles. In 1932, Lennard–Jones predicted that the vdW interaction of neutral atoms and molecules with solid surfaces is governed by a potential of the form

$$V(r) = -\frac{C_3}{r^3}, \tag{1}$$

where r is the distance between the atom and the surface and C_3 is a material-dependent constant. The expression is valid provided that $r \gtrsim 1$ nm [18] and as long as r is not so large that retardation effects become important [19]. In the wave picture, this potential induces a phase [20] shift approximately given by

$$\phi(r) = -\frac{V(r)d}{\hbar v}, \tag{2}$$

where d is the interaction length (which we here assume to be equal to the grating thickness), v is the beam velocity and $\hbar$ is the reduced Planck constant. In the particle picture, the interaction is represented by the force F deflecting the particle in the disc shadow,

$$F(r) = -\frac{\mathrm{d}V}{\mathrm{d}r} = -\frac{3C_3}{r^4}. \tag{3}$$

Since the force is radially pointing inwards from the rim of the circular object, all particles that get accelerated enough to compensate for any velocity away from the optical axis will be on a trajectory intercepting the optical axis. This results in a spot of diverging intensity at the center of the shadow similar to the Poisson spot in the wave picture that has intensity equal to the undisturbed wave front. However, in any real experiment, the circular object will deviate from a perfect circular shape and exhibit a roughness at the edge. In [11], we have already shown that it is necessary to include disc-edge roughness to account for the intensity variation in experimental Poisson spot measurements. Here, we show that in the particle picture, the disc-edge roughness has an even stronger damping effect on the diverging intensity spot. Furthermore, the edge roughness quickly becomes less important in the wave picture as one moves the imaging plane away from the circular object. Unfortunately, it is possible that the bright spot due to particle deflection becomes more intense with increasing distance between the disc and image plane (b) so that simply measuring the intensity as a function of b is not enough to discriminate between the particle and the wave. However, it is possible to distinguish between the two pictures by measuring the intensity of the bright spot from circular objects with different amounts of known edge roughness Δr. The edge roughness can be measured experimentally beforehand in an electron microscope and to some extent controlled during fabrication of the circular object.

2. Poisson's spot with molecules: deuterium and C_{70}

To justify the statement above, we compare a Fresnel diffraction model, which we have adapted to include a vdW phase term, to a simple classical deflection model. We account for edge roughness in both models and use them to simulate both the Poisson spot experiment with deuterium that we have already published [11] and a hypothetical Poisson spot experiment with the fullerene C_{70}.

For the deuterium beam, we use the same setup and parameters as in our experiment in [11]. The supersonic expansion beam had a nozzle temperature of $T_0 = 101$ K and a nozzle pressure of $p_0 = 10$ bar. The nozzle diameter was 10 μm. This resulted in a beam with a most probable

velocity of $v_{\mathrm{deut}} = 1060\,\mathrm{m\,s^{-1}}$, which corresponds to a de Broglie wavelength of $\lambda_{\mathrm{deut}} = 96\,\mathrm{pm}$. The source-to-disc distance was $g = 1496\,\mathrm{mm}$ and we measured the intensity at disc-to-image distances of $b = 321$, 641 and 801 mm. The strength of the vdW interaction between deuterium and SiN was determined in a grid diffraction experiment by Grisenti *et al* [18], where they determined $C_3 = 0.33 \pm 0.09\,\mathrm{meV\,nm^3}$. The disc radius was $R = 30\,\mu\mathrm{m}$ with a disc edge roughness of about 300 nm, and the disc thickness was approximately $d = 1\,\mu\mathrm{m}$.

For the C_{70} scenario, we consider beam properties published in [21]. C_{70} has an atomic mass of 840 amu, which corresponds to a de Broglie wavelength of $\lambda_{C_{70}} = 2.2\,\mathrm{pm}$ at a molecular speed of $v_{C_{70}} = 215\,\mathrm{m\,s^{-1}}$. For the calculations, we assume a source-to-disc distance of $g = 1000\,\mathrm{mm}$ and disc-to-image distances of $b = 250$, 500 and 1500 mm. The vdW constant is estimated with $C_3 = 90\,\mathrm{meV\,nm^3}$ in [21] based on the polarizability of C_{70} and the assumption that the disc is made of gold. We also assume a smaller disc radius of $R = 5\,\mu\mathrm{m}$ with a disc edge roughness of 30 nm and a disc thickness of $d = 50\,\mathrm{nm}$. It is reasonable to assume that a free-standing disc with such parameters can be fabricated using modern electron-beam lithography processing. We have recently demonstrated [22] that free-standing zone plates with a diameter of 388 μm and a thickness of about 150 nm can be produced successfully using electron-beam lithography and a silicon nitride membrane.

2.1. The wave model versus the particle model

The wave diffraction model we have used in this paper is the same as the one we used for the deuterium Poisson spot experiment [11] except that it has been modified to include the vdW phase in equation (2). We calculate the disturbance caused at the point P_1 in the image plane in Fresnel approximation and in polar coordinates by numerically solving the integral [23],

$$U(P_1) = -\frac{\mathbf{i}}{\lambda}\frac{A\,\mathrm{e}^{\mathbf{i}k(g+b)}}{gb}\iint f(r,\theta)\mathrm{e}^{\mathbf{i}\pi/\lambda(1/g)+(1/b)r^2}r\,\mathrm{d}r\,\mathrm{d}\theta, \tag{4}$$

where the factor $\frac{\mathbf{i}}{\lambda}$ is due to the inclination factor at small angles. The term $\frac{A\,\mathrm{e}^{\mathbf{i}k(g+b)}}{gb}$ is the disturbance that would be present at the image plane without an aperture. The surface integral is performed in the aperture plane over the open areas of the general aperture, as described by the aperture function $f(r,\theta)$. It equals 1 if the point (r,θ) is transparent and 0 otherwise. Here, g and b are the distances from the source to the aperture and from the aperture to the image plane, respectively.

The integral can be evaluated efficiently, as described in [23], if the arbitrary aperture is either completely transparent or completely opaque at any one place. Further, one can make use of the rotational symmetry as in the case of a circular obstacle to increase efficiency. The computation essentially becomes a sum over line integrals. The line integrals are along rays in the aperture plane that originate at the point where the source-to-P_1 line passes through the aperture plane. The line integrals can be solved analytically, turning the integral into a sum of phasors (two for each open area the ray traverses). So, all that needs to be calculated are the intersection points of the rays with the disc edges, which can also be expressed analytically (the intersection of a line with a circle).

In this model, we have also accounted for the vdW phase given in equation (2) by adding it to the exponent in equation (4),

$$U(P_1) = -\frac{\mathbf{i}}{\lambda}\frac{A\mathrm{e}^{\mathbf{i}k(g+b)}}{gb}\iint f(r,\theta)\mathrm{e}^{\mathbf{i}\pi/\lambda((1/g)+(1/b))r^2+\mathbf{i}\phi(r)}r\,\mathrm{d}r\,\mathrm{d}\theta. \tag{5}$$

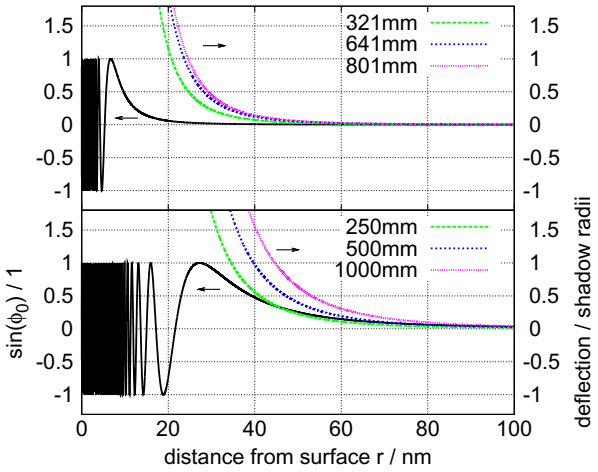

Figure 1. The top and bottom panels show the oscillation of the sine of the vdW phase as a function of distance from the disc edge for the deuterium and C_{70} cases, respectively. The deflection of the molecules based on the particle model are also shown as a function of distance from the disc edge and in units of the radius of the shadow in the image plane. Hence, the particle's trajectories intersect the optical axis in the image plane when deflection is equal to one in this graph. This helps us to visualize at what distance from the rim the particles contribute to the classical on-axis spot. Note also how the region where the vdW forces cause phase changes in the C_{70} experiment extends much further away from the disc edge. Finally, also note that the classical forces acting on the C_{70} molecules are stronger due to their larger polarizability. However, the amount of deflection is also compensated for by their larger mass.

This makes the line integrals mentioned in the previous paragraph more complex to solve, requiring a numerical integration at a computationally expensive step in the algorithm. We therefore computed the line integrals only in a ring surrounding the disc and neglected the contribution from the vdW phase outside of that ring. For the deuterium simulation, this ring had a width of 1 μm, and in the C_{70} simulation it was 2 μm wide. As can be seen in figure 1, the vdW phase shift is close to zero even at 100 nm distance. Hence, this is a good approximation.

As is already known [12], the intensity of the Poisson spot increases due to the phase contribution of the vdW force. This can be understood also by looking at the phase plot in figure 1. The phase contribution oscillates so that for some distances r, the phase is changed so that positive interference is increased on the optical axis. This is also how a phase zone plate works, except that the nth radius r_n where the phase contribution switches from positive to negative is proportional to $n^{-1/3}$ instead of $n^{1/2}$ for a normal zone plate [24], which one can deduce by requiring that the phase shift $\phi(r)$ is a multiple n of $\pi/2$,

$$\frac{C_3 d}{\hbar v r^3} \stackrel{!}{=} n\frac{\pi}{2}. \tag{6}$$

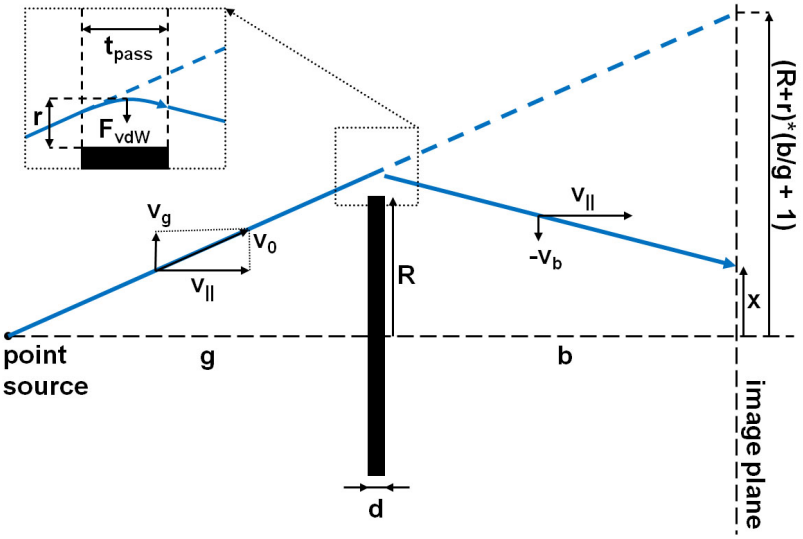

Figure 2. Schematic diagram of the Poisson spot experiment and notation for the classical deflection model.

For the inner edge of a circular aperture, the trend would be even in the same direction as for a phase zone plate. In other words, in that case we have a decreasing zone width with an increasing radius (and a decreasing distance to the inner edge). We therefore conclude that a sufficiently small aperture can be used to focus neutral matter waves to some extent provided that the vdW interaction is strong enough.

We move on to simulate the particle picture. Here, we use a Monte Carlo type algorithm to calculate the number of deuterium molecules that would be classically deflected into the shadow of the disc. The notation we use is explained in figure 2. The force exerted on each particle as it passes the region close to the disc edge is given by equation (3). Since the interaction time is very short compared to the total flight time,

$$t_{\text{pass}} \approx \frac{d}{v_{\parallel}}. \tag{7}$$

All we have to calculate is a change in vertical velocity,

$$-v_b = F(r)/m \times t_{\text{pass}} = -\frac{3C_3 d}{r^4 m v_{\parallel}}, \tag{8}$$

where m is the particle mass and $v_{\parallel}$ is the particle's velocity along the optical axis, which we estimate with v_0 in this paper, since g and b are large compared to $R+r$. Thus, the final position in the imaging plane is given by

$$x = (R+r)(1+b/g) - \frac{3C_3 db}{r^4 m v_{\parallel}^2}. \tag{9}$$

The disc edge roughness included in both models is a fourth power sine extending the rim of the disc with a period of approximately 1 μm in the case of deuterium and 167 nm for C_{70}.

We have used the fourth power of a sine to make the protrusions from the edge sharper, which makes them more similar to the edge roughness we actually observed in scanning-electron microscopy images. A further improvement of the model could use a randomized edge roughness or use the actual imaged edge roughness at the cost of increased computation time. We have used the periodic sine function because it was easier to implement and we judged it to be a reasonably good approximation.

When solving the Fresnel integral, we numerically find the intersections of the corrugated edge with the ray along which we have to integrate. When calculating the vdW phase, we assume that the molecule is interacting with a surface plane that is tangential to the disc edge. The roughness is modeled by taking into account the changed distance to the edge. A more thorough model might derive the potential as a function of position in the disc plane using finite-element analysis.

In the case of the particle deflection, we simply remove the particles that are blocked by the corrugated edge. The direction of the new force vector for those particles that pass the disc close to the corrugated edge is found numerically by summing the vectors from the point where the particle intersects the disc plane to equally spaced points on the corrugated edge. In the simulation, we used 100 points per period, which we found to be a good compromise between model accuracy and computation times. The vectors that intersect the corrugated edge are not included in this summation to simulate the shadowing effect of the roughness. The absolute force is estimated by finding the distance of the corrugated edge in the new direction, which is also not ideal but a good approximation due to the strong decrease with distance of the vdW force.

2.2. Results

The results of the Fresnel integration for our two case studies are shown in figures 3 and 4. The plots show the point spread function (PSF) of the discs for the three different disc-to-image distances b mentioned earlier. The data we can expect to measure would be further convoluted with the source size (incoherent source) and the finite detection area. The graphs also show the expected relative intensities for different amounts of edge roughness. The most important point to note is that the effect of edge roughness changes from halving the Poisson spot intensity at the smallest b-value to almost not affecting it at the largest value of b.

In figures 5 and 6, we present the results for the PSFs from the classical particle deflection model for the deuterium and C_{70} experiments, respectively. The results with 0 nm roughness were calculated with a 30×30 nm pixel size. This means that the data point on the optical axis corresponds to the ratio of particles passing through a pixel centered on the optical axis to the number of particles passing through a pixel outside of the shadow. For the data corresponding to higher roughness, we used 60 nm square pixels. This finite pixel size is the reason why the graph does not completely diverge to infinity in the 0 nm roughness case. Each of the graphs is the result of a simulation of 10^8 or 10^9 particles passing through a 2 μm-wide ring area adjacent to the disc.

We note that in the particle model, the attenuation due to the edge roughness is almost independent of how far behind the disc we sample the image. This is mainly due to the vdW force's strong dependence on distance. The point on the edge that is closest to the particle contributes the most to the attractive force and therefore can easily deflect the particle on to a trajectory that does not pass through the optical axis of the experiment. However, as mentioned

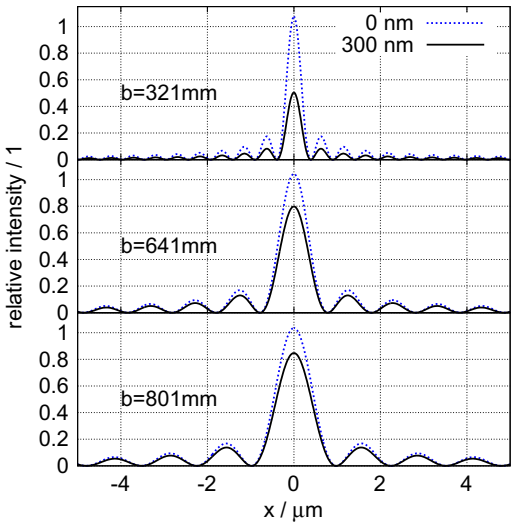

Figure 3. The Poisson spot's lateral intensity distribution for the case of the deuterium experiment assuming a point source and point detector. The length values in the legend refer to the peak-to-peak roughness accounted for in the calculation. The top, middle and bottom panels correspond to disc-to-image distances of $b = 321$, 641 and 801 mm, respectively. The simulated beam has a de Broglie wavelength of 96 pm and the 30 μm-radius disc is at a distance of $g = 1496$ mm from the source.

before and as we can see especially in figure 6, the intensity in the ideal disc case increases with distance b. Therefore, showing an increase in spot intensity as a function of b with respect to the undisturbed beam intensity is not enough to conclude that the wave model is valid. (The intensity behind the disc is also modulated by the $1/(g+b)^2$ dependence of beam intensity and also due to the magnification factor g/b that results from imaging an incoherent source.) However, it is possible to record the intensity of the spot from discs with different amounts of edge roughness and show that the intensity variation corresponds to that calculated with the wave model.

It is interesting to look at the phase shift due to the vdW potential and compare this to the amount of particle deflection as a function of the distance r from the disc edge. This is visualized in figure 1. Note how the region that affects the phase of the molecule is much wider in the C_{70} case and starts to overlap the region where the particles are deflected towards the optical axis. The deflection is given in units of the shadow radius in the image plane. Hence, if the deflection is 1 in the graph, the particle intersects the optical axis at the corresponding value of b.

In a realistic Poisson spot experiment, we have to also take into account that we have to deal with incoherence of the source and the finite size of the detector. To answer the question whether a Poisson spot experiment with C_{70} is possible with current methods, we first look at the center line intensity $I(0)$ of an effusive source [25],

$$I(0) = 1.125 \times 10^{22} \frac{p_0}{\sqrt{MT}} \sigma \left[\frac{\text{molecules}}{\text{sr s}} \right]. \tag{10}$$

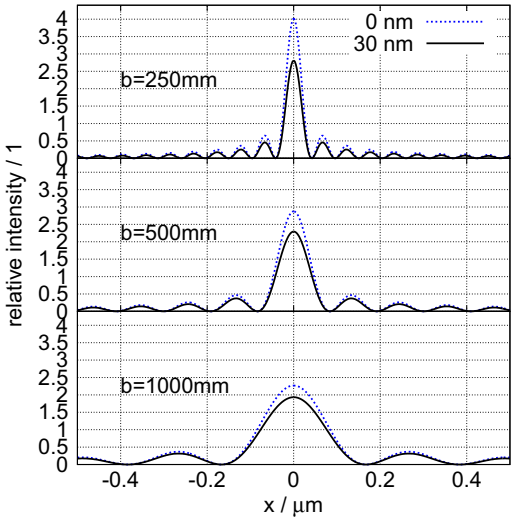

Figure 4. The Poisson spot's lateral intensity distribution for the case of the C_{70} experiment assuming a point source and a point detector. The length values in the legend refer to the peak-to-peak roughness accounted for in the calculation. The top, middle and bottom panels correspond to a disc-to-image distance of $b = 250$, 500 and 1000 mm, respectively. The simulated beam has a de Broglie wavelength of 2.2 pm and the 5 μm-radius disc is at a distance of $g = 1000$ mm from the source.

Here, p_0 is the pressure within the source in torr and σ is the area of the source orifice in square centimeters. M is the molecular weight and T the temperature of the gas or vapor inside the source. An effusive C_{70} source at a temperature $T = 900$ K will have a pressure of approximately 2 Pa [26].

Then we have $I(0) \approx 10^{11}$ molecules sr $^{-1}$ s^{-1} for our chosen parameters and an 8 μm-diameter source orifice. The brightness of the effusive source is thus about 2×10^{21} molecules sr^{-1} s^{-1} m^2, which compares to about 10^{28} molecules sr^{-1} s^{-1} m^2 for the supersonic expansion deuterium source [27]. This huge difference is, however, reduced when taking into account that the detection efficiency of molecular beams is 10^{-5} while for C_{60} a value close to unity has been reported [16]. Moreover, the background in the vacuum chamber at the same mass of the probed molecules contributes to noise and at mass 840 this background will be very close to zero, so also a signal of very low count rate can be measured with C_{70}. Therefore, if we assume similar collimation in the incident beam and similar acceptance angle of the detector, the two experiments have the same feasibility. Unfortunately, for C_{70} the wavelength is smaller and the size of the disc has to be reduced. We have reduced the size of the disc in the C_{70} example simulated in this paper, but more ideally the experiment would be optimized also with smaller g and b to mitigate the reduction in the solid angles. In the present calculation, considering the worst case, we have not tried to optimize the setup and we have used a similar geometrical distance for deuterium and C_{70}.

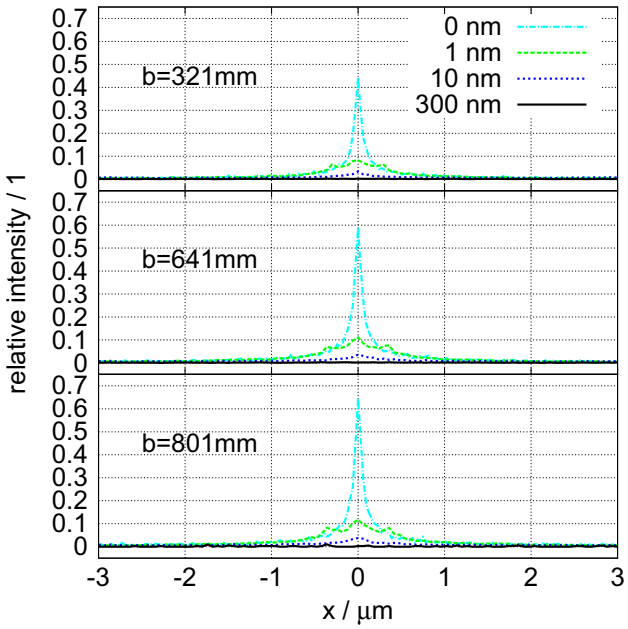

Figure 5. The on-axis bright spot due to classical deflection of the deuterium molecules at the rim of the disc. The top, middle and bottom panels correspond to a disc-to-image distance of $b = 321$, 641 and 801 mm, respectively. The different curves correspond to the peak-to-peak edge roughness given in the legend. The simulated beam had a speed of $1060\,\mathrm{m\,s^{-1}}$ and the $30\,\mu$m radius disc is at a distance of $g = 1496$ mm from the source.

If we use a $4\,\mu$m-diameter detector aperture to record the bright spot, we can expect a flux of approximately 1 particle s^{-1} through it if it is mounted at a distance from the source of $g + b = 1.25$ m. The intensity of the Poisson spot is proportional to the square of the width of the PSF, reducing the measurable intensity by a factor of 100. Also, the Poisson spot in the deuterium experiment was about a factor of 100 less than the undisturbed wave front. So, in total, we expect one particle in 10 000 seconds to deposit in the Poisson spot. The vdW phase increases the intensity of the Poisson spot by almost a factor of 4, as shown in figure 1, but such low count rates would be very challenging to measure, and the improvements suggested above are necessary for the success of the experiment. In addition, one could also attempt to coherently increase the wavelength of the C_{70} molecules by slowing them down; for example, using an atomic paddle [28], or by increasing the brightness of the effusive source by increasing its temperature.

From this, we can conclude that the scaling to larger molecular masses is not as favorable as, for example, in the case of the Talbot–Lau–Kapitza–Dirac grating-based experiments, where a scalability of up to 10^6 atomic mass units is expected [14]. We expect that the above-discussed experiment with C_{70} is close to the limit of what is feasible with current beam sources and detectors. Nevertheless, studying the Poisson spot with large molecules could give new insights

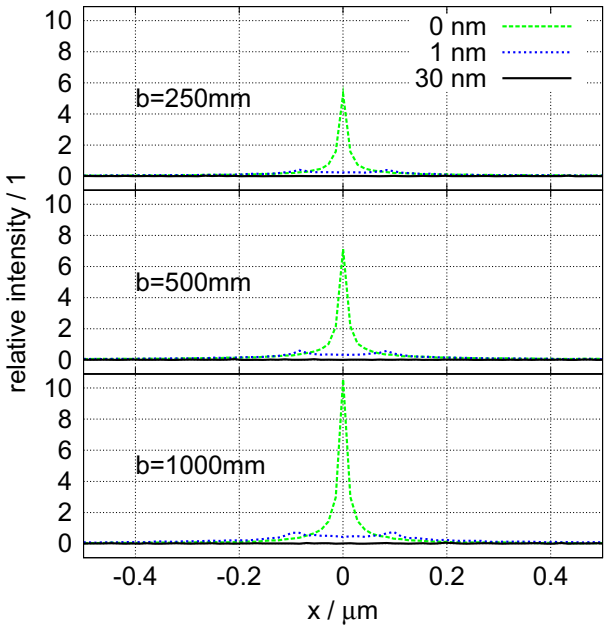

Figure 6. The on-axis bright spot due to classical deflection of the C_{70} molecules at the rim of the disc. The top, middle and bottom panels correspond to disc-to-image distances of $b = 250$, 500 and 1000 mm, respectively. The different curves correspond to the peak-to-peak edge roughness given in the legend. The simulated beam had a speed of 215 m s^{-1} and the 5 μm-radius disc is at a distance of $g = 1000$ mm from the source.

into the interaction potential between molecules and a wall represented by the disc edge. We have described this interaction using the vdW potential given in equation (1) and we noted that this potential can lead to an increase in the observed Poisson spot intensity. At distances roughly equal to or larger than the characteristic absorption wavelength, the dispersion force potential is more accurately described by the Casimir–Polder potential [29]. In the Poisson spot experiment, we expect this long-range interaction to also contribute to the intensity of the Poisson spot, whereas in grating-based experiments this would be canceled out by the potential from the next adjacent grating bar. Furthermore, it would be interesting to study using the Poisson spot intensity the dependence of the Casimir–Polder potential on edge roughness or periodic corrugations, which is nontrivial and a subject of ongoing research [30].

3. Conclusion

We have presented a wave diffraction model and a classical deflection model for the on-axis bright spot from a disc with a certain edge roughness. We applied the models to our already performed deuterium Poisson spot experiment that has already been realized and to a hypothetical experiment with C_{70}. The attenuation effect on the central spot in the shadow of the

disc is much more pronounced in the particle model, and the attenuation is reduced significantly in the wave picture as one moves the imaging plane away from the disc. We therefore propose that this difference between the two models could be used to distinguish between wave and particle behaviors in quantum mechanical experiments with large molecules. We also estimated whether a Poisson spot experiment with C_{70} molecules can be performed with state-of-the-art equipment. The answer is that with a sufficiently bright source, a sufficiently efficient detector and optimized parameters, this could be achieved, but we note that the scaling to smaller de Broglie wavelengths is not very favorable in the case of the Poisson spot experiment. However, we believe that a Poisson spot experiment with large molecules could give new insights into the study of the Casimir–Polder interaction.

Acknowledgments

This work was supported by Bergen's Research Foundation. GB acknowledges support from the Michelsen Centre for Industrial Measurements Science and Technology (MIMT), Norway.

References

[1] Sommerfeld A 1978 Optik *Vorlesungen über Theoretische Physik* vol 4 (Frankfurt: Harri Deutsch)
[2] Born M and Wolf E 1999 *Principles of Optics* (Cambridge: Cambridge University Press)
[3] de Broglie L 1923 Waves and quanta *Nature* **112** 540
[4] Davisson C and Germer L 1927 Diffraction of electrons by a crystal of nickel *Nature* **119** 558
[5] Möllenstedt G and Düker H 1956 Beobachtungen und Messungen an Biprisma-Interferenzen mit Elektronenwellen *Z. Phys.* A **145** 377–97
[6] Kearney P D, Klein A G, Opat G I and Gähler R 1980 Imaging and focusing of neutrons by a zone plate *Nature* **287** 313–4
[7] Carnal O, Sigel M, Sleator T, Takuma H and Mlynek J 1991 Imaging and focusing of atoms by a Fresnel zone plate *Phys. Rev. Lett.* **67** 3231–4
[8] Doak R B, Grisenti R E, Rehbein S, Schmahl G, Toennies J P and Wöll Ch 1999 Towards realization of an atomic de Broglie microscope: helium atom focusing using Fresnel zone plates *Phys. Rev. Lett.* **83** 4229–32
[9] Koch M, Rehbein S, Schmahl G, Reisinger T, Bracco G, Ernst W E and Holst B 2008 Imaging with neutral atoms—a new matter–wave microscope *J. Microsc.* (cover story) **229** 1
[10] Reisinger T and Holst B 2008 Neutral atom and molecule focusing using a Fresnel zone plate *J. Vac. Sci. Technol.* B **26** 2374–9
[11] Reisinger T, Patel A A, Reingruber H, Fladischer K, Ernst W E, Bracco G, Smith H I and Holst B 2009 Poisson's spot with molecules *Phys. Rev.* A **79** 053823
[12] Juffmann T, Nimmrichter S, Arndt M, Gleiter H and Hornberger K 2010 New prospects for de Broglie interferometry *Found. Phys.* at press arXiv:1009.1569v1 [quant-ph]
[13] Arndt M, Nairz O, Vos-Andreae J, Keller C, van der Zouw G and Zeilinger A 1999 Wave–particle duality of C_{60} molecules *Nature* **401** 680–2
[14] Gerlich S *et al* 2007 A Kapitza–Dirac–Talbot–Lau interferometer for highly polarizable molecules *Nat. Phys.* **3** 711–5
[15] Cronin A D, Schmiedmayer J and Pritchard D E 2009 Optics and interferometry with atoms and molecules *Rev. Mod. Phys.* **81** 1051–129
[16] Juffmann T, Truppe S, Geyer P, Major A G, Deachapunya S, Ulbricht H and Arndt M 2009 Wave and particle in molecular interference lithography *Phys. Rev. Lett.* **103** 263601
[17] Gerlich S, Gring M, Ulbricht H, Hornberger K, Tüxen J, Mayor M and Arndt M 2008 Matter–wave metrology as a complementary tool for mass spectrometry *Angew. Chem. Int. Ed. Engl.* **47** 6195–8

[18] Grisenti R E, Schöllkopf W, Toennies J P, Hegerfeldt G C and Köhler T 1999 Determination of atom–surface van der Waals potentials from transmission-grating diffraction intensities *Phys. Rev. Lett.* **83** 1755–8
[19] Hornberger K, Sipe J E and Arndt M 2004 Theory of decoherence in a matter wave Talbot–Lau interferometer *Phys. Rev.* A **70** 053608
[20] Perreault J D and Cronin A D 2005 Observation of atom wave phase shifts induced by van der Waals atom–surface interactions *Phys. Rev. Lett.* **95** 133201
[21] Brezger B, Hackermüller L, Uttenthaler S, Petschinka J, Arndt M and Zeilinger A 2002 Matter–wave interferometer for large molecules *Phys. Rev. Lett.* **88** 100404
[22] Reisinger T, Eder S, Greve M M, Smith H I and Holst B 2010 Free-standing silicon-nitride zoneplates for neutral-helium microscopy *Microelectron. Eng.* **87** 1011–4 (*35th Int. Conf. on Micro- and Nano-Engineering (MNE)*)
[23] Dauger D E 1996 Simulation and study of Fresnel diffraction for arbitrary two-dimensional apertures *Comput. Phys.* **10** 591–604
[24] Hecht E 2002 *Optics* 4th edn (Reading, MA: Addison-Wesley)
[25] Pauly H 1988 *Atomic and Molecular Beam Methods* vol 1 (Oxford: Oxford University Press) p 14
[26] Piacente V, Gigli G, Scardala P, Giustini A and Bardi G 1996 Vapor pressure of C_{70} fullerene *J. Phys. Chem.* **100** 9815–9
[27] Miller D R 1988 *Atomic and Molecular Beam Methods* vol 1 (Oxford: Oxford University Press) p 14
[28] Narevicius E, Libson A, Riedel M F, Parthey C G, Chavez I, Even U and Raizen M G 2007 Coherent slowing of a supersonic beam with an atomic paddle *Phys. Rev. Lett.* **98** 103201
[29] Casimir H B G and Polder D 1948 The influence of retardation on the London–van der Waals forces *Phys. Rev.* **73** 360–72
[30] Klimchitskaya G L, Mohideen U and Mostepanenko V M 2009 The Casimir force between real materials: experiment and theory *Rev. Mod. Phys.* **81** 1827–85